Taming Phosphorus Mononitride

André K. Eckhardt, ¹ Martin-Louis Y. Riu, ¹ Mengshan Ye, ¹ Peter Müller, ¹ Giovanni Bistoni, ^{2, 3} and Christopher C. Cummins ^{1, *}

Keywords: Azide – Phosphorus – Small Molecule Activation – Thermolysis – Transition Metal Chemistry

Abstract. Phosphorus mononitride (PN) only has a fleeting existence on Earth, and molecular precursors for a mild release of this molecule in solution have remained elusive. Here we report the synthesis of an anthracene-based precursor — an anthracene moiety featuring an azidophosphine bridge across its central ring — that dissociates into dinitrogen, anthracene and PN in solution with a first-order half-life of roughly 30 min at room temperature. Heated under vacuum, this azidophosphine—anthracene decomposes in an explosive fashion at around 42 °C as demonstrated in a molecular beam mass spectrometry (MBMS) study. The precursor is also shown to serve as a PN transfer reagent in the synthesis of a Fe–NP coordination complex, through ligand exchange with its Fe–N₂ counterpart. The terminal N-bonded complex was found to be energetically preferred, compared to its P-bonded linkage isomer, owing to a significant covalent Fe–pnictogen bond character and an associated less unfavorable Pauli repulsion in the metal–ligand interaction.

The dinitrogen analogue phosphorus mononitride (PN) is the first phosphorus containing compound detected in the interstellar medium in 1987.^{1,2} On Earth, PN was first accidentally prepared in a discharge through air in a tube, which previously had been used with phosphorus by Herzberg *et al.* in 1933 and spectroscopically characterized based on 24 rotational bands.³ Previously Moldenhauer already reported the formation of a remarkably stable yellow powder in a discharge through nitrogen and phosphorus with a stoichiometry of equal amounts of phosphorus and nitrogen.⁴ Alternatively, monomeric PN is formed in the high-vacuum flash pyrolysis of P₃N₅ at 800–900 °C, isolated in solid krypton at 10 K, and characterized based on its single infrared fundamental at 1323 cm^{-1,5} In the absence of a noble gas matrix PN polymerizes to [PN]_n and aromatic cyclotriphosphazene ((PN)₃), which also forms in electron irradiation experiments of ammonia (NH₃) and phosphine (PH₃) containing ices⁶ at cryogenic temperatures.⁷ The cyclotriphosphazene molecule undergoes a photochemically induced rearrangement to its Dewar benzene-type valence isomer. Under matrix isolation conditions

¹ Department of Chemistry, Massachusetts Institute of Technology, Cambridge MA, USA

² Max-Planck-Institut für Kohlenforschung, Kaiser-Wilhelm-Platz 1, 45470 Mülheim an der Ruhr, Germany

³ Present address: Department of Chemistry, Biology and Biotechnology, University of Perugia, 06123 Perugia, Italy

^{*} E-mail: ccummins@mit.edu

PN was reported to interact with different metal atoms, including Cu, Ag, Au, Co, Ni and Pd.⁸ *Ab initio* computations indicate that PN is thermodynamically unstable and formation of N₂ and diphosphorus (P₂) is exergonic.⁹ Klapötke *et al.* described with P₃N₂₁ the smallest structurally characterized discrete binary PN molecule so far.¹⁰

The stabilization and activation of dipnictogens, e.g., N₂, ¹¹ P₂, ¹², ¹³ and just recently PN¹⁴ is still an ongoing endeavor in inorganic chemistry. Due to its high reactivity and the absence of a suitable molecular precursor for a mild release of PN, molecules containing embedded phosphorus mononitride units have been synthesized and stabilized in various fashions, e.g., N-heterocyclic carbenes, 15 anthracene (1, A), 16 or cyclo-tetraphosphazene. 17 Niecke and coworkers reported with iminophosphenium tetrachloroaluminate (2, Figure 1 top left) the first stable compound with a PN triple bond of 1.475(8) Å according to a crystallographic study. 18 The Bertrand group reported the stabilization of PN by two N-heterocyclic carbenes (3, Figure 1 top middle). 15 However, the central P-N interatomic distance was reported in the crystal structure as 1.709(2) Å, which is significantly longer than the triple bond in the gaseous PN molecule determined by microwave spectroscopy to be 1.49086(2) Å.¹⁹ Hence, a better description for the compound would be R'R''C=P-N=CR₂ instead of R'R''C \rightarrow P=N \leftarrow CR₂.²⁰, ²¹ A similar result was observed by doubly anthracene stabilized PN in APNA (4, Figure 1 top right). However, from none of these PN-containing complexes could free molecular PN be released, yet. Even the isolation of metal complexes with a PN ligand seems to be challenging because of rapid oligomerization reactions as demonstrated by the phosphinidene reactivity of the transient $PNV(N[^tBu]Ar)_3$ (Ar = 3,5-Me₂C₆H₃) complex.²² Only just recently, Martinez et al. reported the synthesis of the first crystallographically characterized PN transition metal complex, namely $[(N_3N)Mo-P\equiv N]^-$ ($[Mo](PN)^-$, 5), $N_3N = [(Me_3SiNCH_2CH_2)_3N]^{3-}$, which undergoes light-induced linkage isomerization to provide $[(N_3N)Mo-N\equiv P]^-([Mo](NP)^-, 6)$, as revealed by photocrystallography (Figure 1, bottom). ¹⁴ The mononuclear PN complex was released in a reaction of tert-butyl isocyanide (BuNC) with a bridging PN heterodinuclear complex that was initially synthesized in a reductive coupling of iron(IV) nitride and molybdenum(VI) phosphide complexes. 14

Results and discussion

Here we report the synthesis of an anthracene based molecular precursor for the release of molecular PN under standard laboratory conditions. In the $7\lambda^3$ -phosphanorbornadiene derivatives have already served as suitable precursors for the release of small phosphorus bearing molecules with only anthracene as a leaving group and byproduct. 16, 23-26 According to the literature chlorophosphine ClPA (7)²³ was synthesized and stirred with an excess of sodium azide (NaN₃, 5 equiv.) in tetrahydrofuran (THF) at -20 °C. The addition of lithium chloride (LiCl, 2 equiv.) as a phase-transfer catalyst²⁷ to solubilize azide ions through conversion of insoluble NaN3 into soluble LiN3 and NaCl proved to be highly efficient in reducing the reaction time to 7–10 days and a crude yield of azidophosphine N₃PA (8) as a colorless solid of up to 70% after workup (Figure 2a, Supplementary Figure 1-3). Single crystals of N₃PA grown from diethyl ether at -20 °C were characterized in a single crystal Xray diffraction experiment and the molecular structure is depicted in Figure 2b (see also Supplementary Figure 27 and Supplementary Table 3). The structure is in line with a strong infrared band for the azide functional group at 2042 cm⁻¹ (Supplementary Figure 6) and a single signal in the proton decoupled ${}^{31}P\{{}^{1}H\}$ NMR spectrum at δ 180.6 ppm (Supplementary Figure 2) that is split into a triplet in the proton coupled ^{31}P NMR spectrum with a coupling constant to the two bridgehead protons of anthracene of $^{2}J_{PH} = 14.5$ Hz. Isotopically ^{15}N labeled $N_{3}PA$, was synthesized from sodium azide-1- ^{15}N following the same procedure. We obtained a statistical mixture with the ^{15}N isotope bonded to phosphorus as well as at the terminal end of the azide unit. Due to ^{31}P - ^{15}N coupling the signal in the ^{31}P { ^{1}H } NMR is split into a doublet that overlaps with the singlet for the terminal ^{15}N labeled $N_{3}PA$ (Supplementary Figure 4). The singlet is not exactly in the center of the doublet because of the isotopic shift. 28,29 We observed two singlet signals at δ 310 and δ 197 ppm in the ^{15}N NMR for both isotopologues that, however, did not split into doublets (Supplementary Figure 5).

A melting point of N₃PA could not be determined because an explosion occurred at 68 °C. This is in line with the results of our molecular-beam mass spectrometer (MBMS) experiment (Figure 2c); N₃PA was heated under vacuum and the released molecules analyzed by mass spectrometry. We observed a strong increase in signals for PN (m/z = 45), N₂ (m/z = 28) and A (m/z = 178 and smaller fragments) already at around 42 °C in the chromatogram as a single strong peak that is clear evidence for an explosive decomposition. Gaseous PN is reported to polymerize very easily and form white powder coatings on surfaces and spectroscopic windows.³⁰ We assume that the polymerization process might also contribute significantly to the observed explosion in our melting point determination. The surface of the sealed capillary was also covered with a white powder coating after the explosion occurred. Phosphorus triazide (P(N₃)₃) was reported to decompose smoothly in solution at room temperature with liberation of nitrogen, accompanied by the appearance of a strong ³¹P resonance at δ 16.2 ppm and a weaker one at δ 6.2 ppm.^{31, 32} However, these two signals were not assigned at all but an assignment to the free PN molecule could be excluded. Similar to many other reported P(III) azides, N₃PA decomposes smoothly in solution at room temperature under standard conditions.³³ Consequently, we followed the decay of N₃PA in benzene-d₆ by ¹H NMR spectroscopy (Supplementary Figure 21-23, Supplementary Table 1-2). The azide decomposes at 25.0 °C with a first order kinetics half-life of around half an hour ($t_{1/2} = 29.1 \pm 1.6$ min) and no new resonances appear in the ³¹P NMR spectrum. Instead we observed the formation of yellow-orange-brown material in our NMR tube that is line with previously reported PN polymerization products; note that the color of the polymer changes depending on the nitrogen content.^{4,34} We performed kinetic measurements on N₃PA decomposition over the temperature range of 25–55 °C. An Eyring analysis revealed activation parameters of $\Delta H^{\ddagger} = 19.5 \pm 1.7$ kcal mol^{-1} and $\Delta S^{\ddagger} = -8.8 \pm 0.8$ cal mol^{-1} (Supplementary Figure 24). The first-order behavior is indicative of a unimolecular rate-determining step, consistent with fragmentation of N₃PA into N_2 , PN and A.

We calculated the most essential decomposition pathways N₃PA at PBE0-D3(BJ)/cc-pVTZ + Gibbs free energy correction with augmented DLPNO-CCSD(T)/cc-pVTZ single point energies (Figure 3). Two minima for N₃PA were located with the energetically preferred conformer in line with our crystal structure depicted in Figure 2b. In the higher energy conformer the azide group takes a parallel position to a terminal aromatic ring that results in an energy rise of 0.9 kcal mol⁻¹. Both conformers are connected by a low lying transition state TS3 (2.9 kcal mol⁻¹). For the decomposition of N₃PA, two fragmentation pathways have been considered, first: cleavage of dinitrogen from the azide group and the formation of phosphinonitrene³⁵ NPA (TS4 23.3 kcal mol⁻¹ and TS5 39.8 kcal mol⁻¹) that easily further dissociates into PN and A via TS6 (1.7 kcal mol⁻¹). The second pathway is connected with the cleavage of anthracene. In an initial step a phosphirane intermediate (I1) forms *via* TS2 (33.9

kcal mol⁻¹) that further dissociates into N₂, PN and **A** via **TS1** (42.5 kcal mol⁻¹). Based on the computed free energy values the first pathway with an initial cleavage of dinitrogen is energetically favored. The total barrier of the minimum energy decomposition pathway (bold in Figure 3) is 23.3 kcal mol⁻¹ and within the experimental error of our experimental Eyring analysis ($\Delta G^{\ddagger} = \Delta H^{\ddagger} - T\Delta S^{\ddagger} = 22.1 \pm 1.5$ kcal mol⁻¹ at 298.15 K).

PN transfer studies

Next we focused on the ability of N₃PA to serve as a synthon for a PN molecule as a ligand to a transition metal complex. As indicated by our computations (vide supra) the N₃PA molecule has two reactive sites. The reaction may be initiated by cleavage of the azide unit in a Staudinger-type reaction³⁶ with dinitrogen release and the remaining NPA unit might be transferred to a transition metal. On the other hand in our group we had previously demonstrated phosphinidene transfer reactivity of various RPA compounds (including R = Me₂N, Et₂N, Me₂Pip, ⁷Pr₂N).³⁷ Inspired by the recent work of Hamon *et al.*³⁸ as well as Peters and co-workers³⁹ we synthesized $[(dppe)Fe(Cp*)(N_2)][BArF_{24}]$ (9, FeN_2 , dppe =1,2-bis(diphenylphosphino)ethane, $Cp^* = 1,2,3,4,5$ -pentamethylcyclopentadienyl, $BArF_{24} =$ Tetrakis[3,5-bis(trifluoromethyl)phenyl]-borate) by treatment of (dppe)Fe(Cp*)(Cl) with NaBArF₂₄. After stirring the latter two reagents for 60 min in diethyl ether, the initially dark brown solution turned red and a colorless precipitate (NaCl) developed. After filtration through Celite and layering the filtrate with pentane, dark red crystalline blocks formed after one day (Supplementary Figure 12). Note that the color significantly differs from a previously reported yellow solid.³⁹ FeN₂ was characterized by IR, NMR, and Mößbauer spectroscopy as well as single crystal X-ray crystallography (vide infra, Figure 4b, Supplementary Figure 7-11, 25, 28 and Supplementary Table 4). We found a nitrogen-nitrogen bond length of 1.131(7) Å within the single crystal that is only slightly longer than the dinitrogen triple bond in the gas phase (1.09768(5) Å).40

Treatment of FeN₂ with an excess of N₃PA (~3 equiv.) at room temperature in diethyl ether immediately led to a gas evolution and precipitation of anthracene as a colorless solid. After filtration the filtrate was placed in the freezer to crystallize further A that was removed by filtration. The filtrate was layered with pentane. After one day at room temperature dark red crystalline blocks (Supplementary Figure 20) were observed and isolated in 73% yield. The crystals were analyzed by IR, NMR, and Mößbauer spectroscopy as well as single crystal Xray crystallography (vide infra, Figure 4c, Supplementary Figure 13-17, 26, 29 and Supplementary Table 5). Our X-ray crystallographic study revealed the successful formation of [(dppe)Fe(Cp*)(NP)][BArF24] (10, FeNP) with the previously weak N2 ligand replaced by PN (Figure 4c). Surprisingly, the PN ligand is terminally N-bonded to the iron center and displays a PN bond length of 1.493(2) Å that is only slightly longer than in free gaseous PN (1.49086(2) Å, vide supra). Intrinsic bond orbital (IBO)⁴¹ analysis reveals a Wiberg bond order of 2.51 for the PN ligand, which is minimally perturbed vis-a-vis the free PN molecule. The P-N bond distance in **FeNP** is longer than in crystalline [Mes*NP]⁺ salts (Mes* = 2,4,6-'Bu₃C₆H₂), e.g., 1.475(8) Å in 1 or 1.467(4) in [Mes*NP][OTf] (OTf = CF₃SO₃⁻). ^{18, 42} In comparison to [Mo](PN)⁻ the PN distance is approximately 0.043 Å shorter.¹⁴ The Wiberg bond order for PN in [Mo](PN)⁻ is 2.13. IBO charges reveal an almost neutral PN ligand in FeNP (N: -0.57, P: 0.57) in stark contrast to [Mo](PN) where the PN ligand carries an overall significant negative charge (N: -0.95, P: 0.57). This is consistent with the latter system having considerably more back-bonding to the PN ligand (c.f. Figure 5 and Supplementary Figure 34).

The diamagnetic nature of the two prepared transition metal complexes allowed us further spectroscopic characterization by multinuclear NMR spectroscopy. The singlet signal at δ 85 ppm in the $^{31}P\{^{1}H\}$ spectrum of the dppe ligand in FeN_2 (Figure 4d i left, S9) is split into a doublet in FeNP and slightly shifted downfield to δ 86 ppm (Figure 4d i right, Supplementary Figure 15). In addition, a triplet resonance is observed for the NP ligand at δ 271 ppm with a coupling constant of $^{3}J_{PP} = 9.2$ Hz. We synthesized 50% enriched $Fe^{14/15}NP$ by treatment of FeN_2 with ^{15}N labeled $^{15}N_3PA$ (*vide supra*). In the \sim 50% ^{15}N isotopically enriched $Fe^{14/15}NP$ complex the triplet resonance at at δ 271 ppm splits into a doublet of triplets, partially overlapping with the unlabeled triplet (Supplementary Figure 18). A weak doublet at δ 450 pm ($^{1}J_{NP} = 51.1$ Hz) is observed in the ^{15}N NMR spectrum (Supplementary Figure 19). Our attempts to determine the $^{31}P_{-57}$ Fe coupling constant between the PN ligand and the iron center failed. We were only able to determine the coupling constant of the dppe ligand to the ^{57}Fe center to be $^{1}J_{FeP} = 55.4$ Hz in FeN_2 (Supplementary Figure 11) and $^{1}J_{FeP} = 56.5$ Hz in FeN_2 (Supplementary Figure 17).

We collected solid-state infrared (IR) data of all three crystallized complexes (Figure 4d ii) and observed a strong sharp band at 2116.3 cm⁻¹ in **FeN**₂ that is characteristic for a ν_{NN} stretching vibration. The band is not present for the **FeNP** complex. The high wavenumber of 2116.3 cm⁻¹ in comparison to other transition metal dinitrogen complexes is indicative for a weak Fe-N bond. For **FeNP** we observed a shoulder signal at 1270.7 cm⁻¹ that is overlapping with another signal but clearly not present in **FeN**₂. We assign this signal to the ν_{NP} stretching mode that is red shifted by roughly $\Delta \nu = 52$ cm⁻¹ in comparison to free PN ($\nu_{\text{NP}} = 1323$ cm⁻¹).^{5,30} A new band appeared for isotopically labeled **Fe**¹⁵**NP** at 1238.3 cm⁻¹. The experimental isotope shift for the ν_{NP} stretching vibration is $\Delta \nu_{\text{exp}} = 32.4$ cm⁻¹ that is in good agreement with a computed harmonic shift of $\Delta \nu_{\text{calc}} = 34.6$ cm⁻¹ at the PBE0-D3(BJ)/cc-pVTZ level of theory.

We recorded ⁵⁷Fe Mößbauer spectra of FeN₂ and FeNP at 80 K and fitted the data with two Lorentzian functions as included in the WMOSS software (Supplementary Figure 25 and 26).⁴⁴ The spectra of the two complexes show a single doublet which clearly establishes the spectroscopic purity of the samples in line with our other analytical characterization methods (see elemental analysis in Methods section). The line broadening of both complexes ($\Gamma = 0.266$ mm s^{-1} for FeN_2 and $\Gamma = 0.269$ mm s^{-1} for FeNP) is similar to the previously reported [(dppe)Fe(Cp*)][PF₆] complex ($\Gamma = 0.257 \text{ mm s}^{-1}$).³⁸ The isomer shift (δ) for FeN₂ is $\delta = 0.395$ mm s⁻¹ and for FeNP is $\delta = 0.299$ mm s⁻¹. The quadrupole splitting (ΔE_Q) for FeN₂ is $\Delta E_Q =$ 2.018 mm s⁻¹ and for **FeNP** is $\Delta E_0 = 1.696$ mm s⁻¹. The experimental values are in good agreement with our calculations of the corresponding cations; $\delta = 0.409 \text{ mm s}^{-1}$ and $\Delta E_0 =$ 2.008 mm s⁻¹ for FeN₂⁺ (only the cations are considered in our computations and abbreviated in the following with a positive charge) and $\delta = 0.317$ mm s⁻¹ and $\Delta E_0 = 1.712$ mm s⁻¹ for FeNP⁺ (see SI for further details). The experimental difference of roughly 0.1 mm s⁻¹ for the isomer shift is a hint for a greater covalency in FeNP. Similar observations have been reported by the Peters group. In the [K(benzo-15-crown-2)₂][((Ph₂PCH₂SiMe₂)₃CH)Fe(L)] system the isomer shift for L = CO is 0.18 mm s⁻¹ lower than that for $L = N_2$, consistent with stronger CO π backbonding.⁴⁵ Our computed reduced Mulliken (FeN₂⁺: 0.84, FeNP⁺: 0.94) and Löwdin $(FeN_2^+: 0.88, FeNP^+: 0.97)$ orbital charges show a significant higher charge for the Fe d_{yz} orbital for the FeNP⁺ system. The higher orbital charge is related with the experimentally observed lower isomer shift and stronger π backbonding in FeNP (vide infra).

Computational analysis

We explored the potential energy surface around FeNP⁺ computationally. As a global energetic minimum we located a closed shell (S = 0, with S as the total spin number of the system) low spin electronic ground state for the [(dppe)Fe(Cp*)(NP)]⁺ cation (FeNP⁺) at the DLPNO-CCSD(T)/cc-pVTZ//PBE0-D3(BJ)/cc-pVTZ + thermal correction to Gibbs free energy level of theory (Figure 5). Isomerization of the NP ligand occurs via the side-on bound isomer that is connected via TS1 (25.5 kcal mol⁻¹, Figure 5) to FeNP⁺ and 16.8 kcal mol⁻¹ energetically less preferred. Further isomerization via **TS2** (36.6 kcal mol⁻¹, Figure 5) leads to the PN linkage isomer FePN⁺ (11) that is surprisingly 14.3 kcal mol⁻¹ higher in energy than the FeNP⁺ isomer. We computed the ³¹P NMR chemical shifts of all three isomers according to a literature benchmark study at the PBE0-D3(BJ)/6-31G(d) level of theory. 46 According to the computations all three isomers should be distinguishable by NMR spectroscopy as they are separated by roughly 80 ppm (Figure 5). The computed chemical shift for FeNP⁺ with δ 282 ppm is in good agreement with the experimentally observed resonance at δ 271 ppm. The energetic high barrier of **TS2** (36.6 kcal mol⁻¹) prevents isomerization of the NP ligand at room temperature. Even after refluxing the complex in toluene or after irradiation with green and yellow light with light emitting diodes (LEDs) we did not observe any new resonance by ³¹P NMR spectroscopy.

The energetic preference of the FeNP⁺ isomer vs. the FePN⁺ is surprising because we initially expected a better orbital overlap between iron and phosphorus and a preference of the FePN⁺ isomer. However, our local energy decomposition (LED)⁴⁷ and natural orbital chemical valence (NOCV)⁴⁸ analysis indicates that the interaction between the ligand and the metal center is of significant covalent nature (see Figure 5 top for intrinsic bond orbitals (IBOs) and Supplementary Figure 30-33 and Supplementary Table 6-11). In the NOCV/EDA analysis⁴⁹ of **FeNP**⁺ we obtain an energy of -90.8 kcal mol⁻¹ (Table S5) for the orbital interaction term $\Delta E_{\rm orb}$, representing orbital mixing effects, e.g., charge transfer and polarization effects. As the term is similar for FePN⁺ (-98.8 kcal mol⁻¹), this is indicative that the interaction between the ligand and the metal center is strongly covalent in nature and mainly dominated by the ΔE_{steric} term (44.0 kcal mol⁻¹ for FeNP⁺ and 66.8 kcal mol⁻¹ for FePN⁺). The most important mixing contributions for $FeNP^+$ is the π -backdonation from the occupied d orbitals of suitable symmetry on the Fe atom to the empty LUMO antibonding π^* orbitals of the ligand $\Delta E_{\text{orb}}[d(\text{Fe})]$ $\to \pi^*(NP)$] (-28.6 kcal mol⁻¹, Supplementary Figure 33) and $\Delta E_{\rm orb}[d(Fe) \to \pi_{\perp}(NP)]$ (-21.9 kcal mol⁻¹, Supplementary Figure 33). Another significant contribution is the σ -donation from the HOMO of the ligand to the empty d orbitals of Fe $\Delta E_{\rm orb}[\sigma(NP) \rightarrow d(Fe)]$ (-32.1 kcal mol⁻ ¹, Supplementary Figure 33). The relative stability of the isomers correlates well only with Pauli repulsion effects. Thus, the relative stability between the isomers essentially originates from the fact that the atomic orbitals on phosphorus are larger and more diffuse than those on nitrogen. This causes an increase in Pauli repulsion when the ligand coordinates from the phosphorus side. This is not compensated by a corresponding increase in orbital interactions, as quantified by the NOCV scheme (Supplementary Table 11). With a dinitrogen ligand in FeN2+ the orbital interactions are qualitatively the same as in FeNP+. In general, the frontier orbitals of N₂ are of similar shape and nature as in PN (Supplementary Figure 33). However, the LUMO orbitals of N2 feature higher energies than those of PN, whilst the HOMO and HOMO-1 orbitals show lower energies. Hence, N_2 is expected to be a poorer π acceptor as well as a poorer σ donor than PN. This is confirmed by our NOCV/EDA analysis. All donation and back donation components are smaller in $\operatorname{FeN_2}^+(\Delta E_{\operatorname{orb}}[d(\operatorname{Fe}) \to \pi^*(\operatorname{N_2})] = -22.2 \text{ kcal mol}^-$

¹; $\Delta E_{\text{orb}}[d(\text{Fe}) \to \pi_{\perp}(\text{N}_2)] = -18.1 \text{ kcal mol}^{-1}$ and $\Delta E_{\text{orb}}[\sigma(\text{N}_2) \to d(\text{Fe})]$ (-24.1.1 kcal mol⁻¹) than in **FeNP**⁺ (Supplementary Table 11). The covalent interaction between the iron center and the PN ligand is also shown by IBO analysis (Figure 5 top). The backbonding of the metal to the ligand is only minimal (see second row right orbital in Figure 5) and in stark contrast to the situation for [**Mo**](**PN**)⁻ complex reported by the Smith group (Supplementary Figure 34). The Fe–NP *σ*-interaction is represented by the second orbital in the top row of Figure 5. The left orbital in the same row represents the *σ*-bond and the two remaining orbitals on the right the two *π*-bonds of the PN ligand. The two left orbitals in the second row represent *d*-orbitals of the iron center.

Conclusions

In summary, we presented the synthesis and development of a molecular precursor N₃PA that dissociates at room temperature and slowly releases dinitrogen, anthracene and phosphorus mononitride with a half-life of roughly half an hour. Phosphorus mononitride polymerizes very rapidly in solution by forming yellow-orange-brown polymers but can be efficiently transferred and trapped as demonstrated by the synthesis of [(dppe)Fe(Cp*)(NP)][BArF₂₄]. The PN ligand is surprisingly N-bonded to the iron center because of a significant covalent iron pnictogen bond character that results in less Pauli repulsion when the ligand coordinates from the N side. The synthesis of N₃PA and the prepared iron complex with a PN ligand opens new pathways to conduct further reactivity studies of the PN molecule in the future.

Acknowledgements

A.K.E. thanks the Alexander von Humboldt foundation for a Feodor Lynen postdoctoral fellowship. This material is based on research supported by the National Science Foundation, under No. CHE-1955612. We thank all MIT DCIF staff members and Dr. Clemens Anklin (Bruker) for technical support with NMR measurements, as well as Michael C. McCarthy (Harvard CfA), Robert J. Gilliard (University of Virginia) and Daniel L.M. Suess (MIT) for fruitful discussion.

Author contributions

A.K.E. conducted all experiments, carried out the computations of the potential energy surfaces and analyzed the data. M.-L.Y.R. and P.M. collected all diffraction data and refined the structures. M.Y. collected all Mößbauer data. G.B. analyzed the bonding situation in [(dppe)Fe(Cp*)(NP)][BArF24]. C.C.C. administrated the study. A.K.E. wrote the manuscript with input from all authors.

Competing financial interests

The authors declare no competing interests.

Figure 1 | Selected PN containing molecules and transition metal complexes with given PN bond distances. Top: Iminophosphenium tetrachloroaluminate (4, left) as the first stable compound with a PN triple bond (1.475(8) Å). Phosphorus mononitride trapped between two N-heterocyclic carbenes (2, middle) and two molecules of anthracene (APNA, right) with PN bond distances of 1.709(2) Å and 1.691(1) Å, respectively. Selectively. Selection are better described as single bonds. Bottom: Anionic molybdenum complex with a PN ligand that isomerizes by irradiation with white light; The PN bond length in [Mo](PN) (1.5363(1) Å) is only slightly longer than in free PN in the gas-phase (1.49086(2) Å), while the PN bond in [Mo](NP) (1.5913(1) Å) resembles more a N=P double bond, based on the sum of the atomic covalent radii of nitrogen and phosphorous (1.62 Å).

Figure 2 | **Synthesis, structure and decomposition of N₃PA.** a: Synthesis of N₃PA by nucleophilic substitution of ClPA with NaN₃, catalysed by LiCl in THF at -20 °C. N₃PA slowly decomposes at room temperature to PN, N₂ and **A** or in an explosive fashion at elevated temperatures. b: Molecular structure of N₃PA with thermal ellipsoids shown at the 50% probability level. Hydrogen atoms are omitted for the sake of clarity. Selected interatomic distances (Å): P1-N1 1.7643(14); P1-C1, 1.9025(16); P1-C8, 1.8882(15); N1-N2, 1.2341(18); and N2-N3, 1.1325(19). Selected interatomic bond angles (°): C1-P1-C8, 80.15(7); P1-N1-N2, 115.22(11). c: Molecular Beam Mass Spectrometry (MBMS) chromatogram of N₃PA. The compound is heated under vacuum and explodes at around 42 °C based of the strong sharp signal increase of PN, N₂ and **A**. The other detected signals after the main explosion might be explained by several micro explosions.

Figure 3 | Computed decomposition pathways of N₃PA. N₃PA decomposes into N₂, PN and anthracene either by dinitrogen and subsequent anthracene loss with a NPA intermediate (right part of the PES) or via a rearrangement to a phosphirane intermediate (I1) and subsequent concerted dissociation into N₂, PN and anthracene (Left part of the PES). Gibbs free energy values are computed for T = 298.15 K. The minimum energy dissociation path is depicted in bold. The overall reaction barrier is 23.3 kcal mol⁻¹. Color code: carbon = grey, hydrogen = white, nitrogen = blue, phosphorus = orange.

Figure 4 | Synthesis, structure and spectroscopic characterization of FeN₂ and FeNP. a: Synthesis of FeNP by treatment of FeN₂ with N₃PA in diethyl ether at room temperature. After crystallization the complex can be isolated in 73% yield. b and c: Molecular structure of FeN₂ and FeNP with thermal ellipsoids shown at the 50% probability level. Hydrogen atoms are omitted for the sake of clarity. The NP-bond distance in c is 1.493(2) Å and very close to the bond length in gaseous PN (1.49086(2) Å). d: ii: Infrared spectrum of FeN₂ (black), FeNP (red) and Fe^{14/15}NP (blue, ~50% enriched with ¹⁵N). The NN stretching vibration ν_{NN} at 2116.3 cm⁻¹ in the black spectrum is absent in the red and blue spectrum. Due to substitution with a heavier isotopologue the NP stretching vibration is shifted from 1270.7 cm⁻¹ (red spectrum) to 1238.3 cm⁻¹ (blue spectrum). i and iii ³¹P{¹H} NMR spectrum of FeN₂ and FeNP, respectively. The singlet resonance in i of the dppe ligand at 84.53 ppm is split into a doublet in iii at 85.95 ppm due to coupling to the NP ligand, which is represented by the triplet resonance at 271.02 ppm.

Figure 5 | Isomerization of the PN ligand in [(dppe)Fe(Cp*)(NP)]⁺ and analysis of the bonding situation. Top: Selected intrinsic bond orbitals (IBOs): The top row shows the σ_{PN} , the σ_{FeN} , and the two π_{PN} bonds. The bottom row shows the three doubly occupied d orbitals of this d⁶ complex. Note that only in the bottom right orbital there is some weak back bonding. Bottom: Potential energy surface for the isomerization of the PN ligand and computed $^{31}P\{^{1}H\}$ NMR shifts. The total barrier for the complete isomerization is 36.6 kcal mol⁻¹ and proceeds through a side-on bonded FeNP complex. FeNP⁺ is energetically 14.3 kcal mol⁻¹ preferred over FePN⁺. Based on the calculated NMR shifts, all isomers can be easily distinguished by NMR spectroscopy. The calculated NMR shift for FeNP⁺ (282 ppm) is in good agreement with our experimentally observed resonance at 271 ppm. Color code: carbon = grey, hydrogen = white, nitrogen = blue, phosphorus = orange, iron = brown.

References

- 1. Ziurys L. Detection of interstellar PN-the first phosphorus-bearing species observed in molecular clouds. *Astrophys. J.* **321**, L81-L85 (1987).
- 2. Turner B, Bally J. Detection of interstellar PN-The first identified phosphorus compound in the interstellar medium. *Astrophys. J.* **321**, L75-L79 (1987).
- 3. Curry J, Herzberg L, Herzberg G. Spectroscopic Evidence for the Molecule PN. *J. Chem. Phys.* **1**, 749-749 (1933).
- 4. Moldenhauer W, Dörsam H. Über die Vereinigung von Phosphor und Stickstoff unter dem Einflusse elektrischer Entladungen. *Ber. dtsch. Chem. Ges. A/B* **59**, 926-931 (1926).
- 5. Atkins RM, Timms PL. The matrix infrared spectrum of PN and SiS. *Spectrochim. Acta, Part A* **33**, 853-857 (1977).
- 6. Zhu C, Bergantini A, Singh SK, Kaiser RI, Eckhardt AK, Schreiner PR, *et al.* Formation of phosphine imide (HN=PH₃) and its phosphinous amide (H₂N-PH₂) isomer. *Chem. Commun.* **57**, 4958-4961 (2021).
- 7. Zhu C, Eckhardt AK, Bergantini A, Singh SK, Schreiner PR, Kaiser RI. The elusive cyclotriphosphazene molecule and its Dewar benzene–type valence isomer (P₃N₃). *Sci. Adv.* 6, eaba6934 (2020).
- 8. Atkins RM, Timms PL. Interaction of PN with metal atoms in a krypton matrix. *Inorg. Nucl. Chem. Letters* **14**, 113-115 (1978).
- 9. Ahlrichs R, Bär M, Plitt HS, Schnöckel H. The stability of PN and (PN)₃. Ab initio calculations and matrix infrared investigations. *Chem. Phys. Lett.* **161**, 179-184 (1989).
- 10. Göbel M, Karaghiosoff K, Klapötke TM. The First Structural Characterization of a Binary P–N Molecule: The Highly Energetic Compound P₃N₂₁. *Angew. Chem. Int. Ed.* **45**, 6037-6040 (2006).
- 11. McSkimming A, Suess DLM. Dinitrogen binding and activation at a molybdenum–iron–sulfur cluster. *Nat. Chem.* **13**, 666-670 (2021).
- 12. Sun J, Verplancke H, Schweizer JI, Diefenbach M, Würtele C, Otte M, *et al.* Stabilizing P \equiv P: P_2^{2-} , P_2^{-} , and P_2^{0} as bridging ligands. *Chem* 7, 1952-1962 (2021).
- 13. Du J, Hunger D, Seed JA, Cryer JD, King DM, Wooles AJ, *et al.* Dipnictogen f-Element Chemistry: A Diphosphorus Uranium Complex. *J. Am. Chem. Soc.* **143**, 5343-5348 (2021).
- 14. Martinez JL, Lutz SA, Beagan DM, Gao X, Pink M, Chen C-H, *et al.* Stabilization of the Dinitrogen Analogue, Phosphorus Nitride. *ACS Cent. Sci.* **6**, 1572-1577 (2020).
- 15. Kinjo R, Donnadieu B, Bertrand G. Isolation of a Carbene-Stabilized Phosphorus Mononitride and Its Radical Cation (PN⁺). *Angew. Chem. Int. Ed.* **49**, 5930-5933 (2010).
- 16. Velian A, Cummins CC. Facile Synthesis of Dibenzo- $7\lambda^3$ -phosphanorbornadiene Derivatives Using Magnesium Anthracene. *J. Am. Chem. Soc.* **134**, 13978-13981 (2012).
- 17. Hering C, Schulz A, Villinger A. Diatomic PN trapped in a cyclo-tetraphosphazene. *Chem. Sci.* **5**, 1064-1073 (2014).
- 18. Niecke E, Nieger M, Reichert F. Arylmino(halogeno)phosphanes XP=NC₆H₂tBu₃ (X = Cl, Br, I) and the Iminophosphenium Tetrachloroaluminate [P≡NC₆H₂tBu₃]⁺[AlCl4]⁻: the First Stable Compound with a PN Triple Bond. *Angew. Chem. Int. Ed.* **27**, 1715-1716 (1988).
- 19. Wyse FC, Manson EL, Gordy W. Millimeter Wave Rotational Spectrum and Molecular Constants of ³¹P¹⁴N. *J. Chem. Phys.* **57**, 1106-1108 (1972).
- 20. Tofan D, Velian A. Interstellar Chemistry in a Glovebox: Elusive Diatomic P≡N, Exposed. *ACS Cent. Sci.* **6**, 1485-1487 (2020).
- 21. Himmel D, Krossing I, Schnepf A. Dative Bonds in Main-Group Compounds: A Case for Fewer Arrows! *Angew. Chem. Int. Ed.* **53**, 370-374 (2014).
- 22. Courtemanche M-A, Transue WJ, Cummins CC. Phosphinidene Reactivity of a Transient Vanadium P≡N Complex. *J. Am. Chem. Soc.* **138**, 16220-16223 (2016).
- 23. Velian A, Nava M, Temprado M, Zhou Y, Field RW, Cummins CC. A Retro Diels–Alder Route to Diphosphorus Chemistry: Molecular Precursor Synthesis, Kinetics of P₂ Transfer to 1,3-Dienes, and Detection of P₂ by Molecular Beam Mass Spectrometry. *J. Am. Chem. Soc.* 136, 13586-13589 (2014).

- 24. Transue WJ, Velian A, Nava M, Martin-Drumel M-A, Womack CC, Jiang J, *et al.* A Molecular Precursor to Phosphaethyne and Its Application in Synthesis of the Aromatic 1,2,3,4-Phosphatriazolate Anion. *J. Am. Chem. Soc.* **138**, 6731-6734 (2016).
- 25. Transue WJ, Nava M, Terban MW, Yang J, Greenberg MW, Wu G, *et al.* Anthracene as a Launchpad for a Phosphinidene Sulfide and for Generation of a Phosphorus—Sulfur Material Having the Composition P₂S, a Vulcanized Red Phosphorus That Is Yellow. *J. Am. Chem. Soc.* **141**, 431-440 (2019).
- 26. Riu M-LY, Jones RL, Transue WJ, Müller P, Cummins CC. Isolation of an elusive phosphatetrahedrane. *Sci. Adv.* **6**, eaaz3168 (2020).
- 27. Gediga M, Burck S, Bender J, Förster D, Nieger M, Gudat D. Specific and Reversible Alkynyl Transfer Reactions of an N-Heterocyclic Phosphane. *Eur. J. Inorg. Chem.* **2014**, 1818-1825 (2014).
- 28. Hansen PE. Isotope Effects on Nuclear Shielding. In: Webb GA (ed). *Annual Reports on NMR Spectroscopy*, vol. 15. Academic Press, 1984, pp 105-234.
- 29. Hansen PE. Isotope effects in nuclear shielding. *Prog. Nucl. Magn. Reson. Spectrosc.* **20**, 207-255 (1988).
- 30. Ahmad IK, Hamilton PA. The Fourier Transform Infrared Spectrum of PN. *J. Mol. Spectrosc.* **169**, 286-291 (1995).
- 31. Dillon KB, Platt AWG, Waddington TC. The identification of some new azido-derivatives of phosphorus. *Inorg. Nucl. Chem. Letters* **14**, 511-513 (1978).
- 32. Buder W, Schmidt A. Phosphorazide und deren Schwingungsspektren. *Z. Anorg. Allg. Chem.* **415**, 263-267 (1975).
- 33. Gilyarov VA. Phosphorus Acid Azides. Russ. Chem. Rev. 51, 909-920 (1982).
- 34. Holleman AF. *Lehrbuch der anorganischen Chemie*. Walter de Gruyter GmbH & Co KG, 2019.
- 35. Dielmann F, Back O, Henry-Ellinger M, Jerabek P, Frenking G, Bertrand G. A Crystalline Singlet Phosphinonitrene: A Nitrogen Atom-Transfer Agent. *Science* **337**, 1526-1528 (2012).
- 36. Staudinger H, Meyer J. Über neue organische Phosphorverbindungen III. Phosphinmethylenderivate und Phosphinimine. *Helv. Chim. Acta* **2**, 635-646 (1919).
- 37. Transue WJ, Velian A, Nava M, García-Iriepa C, Temprado M, Cummins CC. Mechanism and Scope of Phosphinidene Transfer from Dibenzo-7-phosphanorbornadiene Compounds. *J. Am. Chem. Soc.* **139**, 10822-10831 (2017).
- 38. Hamon P, Toupet L, Roisnel T, Hamon J-R, Lapinte C. Preparation and Characterization of the Triflate Complex [Cp*(dppe)FeOSO₂CF₃]: A Convenient Access to Labile Five- and Six-Coordinate Iron(I) and Iron(II) Complexes. *Eur. J. Inorg. Chem.* **2020**, 84-93 (2020).
- 39. Schild DJ, Drover MW, Oyala PH, Peters JC. Generating Potent C–H PCET Donors: Ligand-Induced Fe-to-Ring Proton Migration from a Cp*Fe^{III}–H Complex Demonstrates a Promising Strategy. *J. Am. Chem. Soc.* **142**, 18963-18970 (2020).
- 40. Huber K-P. *Molecular spectra and molecular structure: IV. Constants of diatomic molecules.* Springer Science & Business Media, 2013.
- 41. Knizia G. Intrinsic Atomic Orbitals: An Unbiased Bridge between Quantum Theory and Chemical Concepts. *J. Chem. Theory Comput.* **9**, 4834-4843 (2013).
- 42. Niecke E, Detsch R, Nieger M, Reichert F, Schoeller W. From covalent to ionic bonding: spontaneous bond dissociation in oxy-substituted iminophosphanes. *Bull. Soc. Chim. Fr.* **130**, 25-31 (1993).
- 43. Kraka E, Freindorf M. Characterizing the Metal–Ligand Bond Strength via Vibrational Spectroscopy: The Metal–Ligand Electronic Parameter (MLEP). In: Lledós A, Ujaque G (eds). *New Directions in the Modeling of Organometallic Reactions*. Springer International Publishing: Cham, 2020, pp 227-269.
- 44. Prisecaru I. WMOSS4 Mößbauer Spectral Analysis Software. 2009-2016, www.wmoss.org (accessed 08-24-2021)
- 45. Rittle J, Peters JC. Fe–N₂/CO complexes that model a possible role for the interstitial C atom of FeMo-cofactor (FeMoco). *Proc. Natl. Acad. Sci. USA* **110**, 15898 (2013).
- 46. Latypov SK, Polyancev FM, Yakhvarov DG, Sinyashin OG. Quantum chemical calculations of ³¹P NMR chemical shifts: scopes and limitations. *Phys. Chem. Chem. Phys.* **17**, 6976-6987 (2015).

- 47. Schneider WB, Bistoni G, Sparta M, Saitow M, Riplinger C, Auer AA, *et al.* Decomposition of Intermolecular Interaction Energies within the Local Pair Natural Orbital Coupled Cluster Framework. *J. Chem. Theory Comput.* **12**, 4778-4792 (2016).
- 48. Mitoraj MP, Michalak A, Ziegler T. A Combined Charge and Energy Decomposition Scheme for Bond Analysis. *J. Chem. Theory Comput.* **5**, 962-975 (2009).
- 49. Altun A, Neese F, Bistoni G. Effect of Electron Correlation on Intermolecular Interactions: A Pair Natural Orbitals Coupled Cluster Based Local Energy Decomposition Study. *J. Chem. Theory Comput.* **15**, 215-228 (2019).
- 50. Pyykkö P, Atsumi M. Molecular Double-Bond Covalent Radii for Elements Li–E112. *Chem. Eur. J.* **15**, 12770-12779 (2009).

Methods

Caution. The handling of azide compounds should be done with the necessary safety precautions.⁵¹ No direct explosions of N_3PA were encountered when it was diluted in organic solvents or carefully dried under vacuum below room temperature. Treatment of transition metal complexes in solution with solid N_3PA can cause a spontaneous explosive decomposition of N_3PA and should be avoided or solid N_3PA only be added in portions of a few milligrams, respectively.

Synthesis of N₃PA (8). Inside the glovebox, a 20 mL vial was charged with solid, colorless ClPA (500 mg, 2.04 mmol, 1.0 equiv.), NaN₃ (675 mg, 10.38 mmol, 5.0 equiv.), LiCl (180 mg, 4.25 mmol, 2.0 equiv.) and a magnetic stir bar. Precooled (-20 °C) THF (15 mL) was added to the vial that was tightly closed with a cap and subsequently transported to the freezer inside the glovebox where it was stirred in the dark for 7 d at -20 °C. After seven days, all volatiles were removed under reduced pressure to yield a cream-colored solid residue. The solids were slurried in diethyl ether (4 x 20 mL) at room temperature and filtered through a celite:charcoal (1:1, 4 cm) plug in a 15 mL medium frit. The colorless ethereal solution was collected in a filter flask that was precooled in the liquid N2 immersed coldwell of the glovebox. Removal of solvent in vacuo from the colorless filtrate left a colorless solid that was weighed and stored in the freezer. Yields varied depending on how much anthracene was produced during the course of the reaction and the workup, giving up to 360 mg (70%) crude product with some anthracene impurities that rapidly decomposes at room temperature yielding a yellowish mixture of anthracene and PN polymers. The identity of the product was confirmed by NMR and IR spectroscopy as well as by an X-ray diffraction study performed on a crystal grown from diethyl ether at -20 °C (Figure 2b). A melting point for this material could not be determined. At 46.0 ± 0.5 °C the compound decomposes in an explosive fashion. DART HRMS(Q-TOF) m/z: [M + H]⁺ Calcd for C₁₄H₁₁N₃P 252.0685; Found 252.0698. ¹H NMR (benzene- d_6 , 400 MHz, 25 °C) δ 7.41 (m, 2H), 7.33 (m, 2H), 7.17(m, 2H), 6.98 (m, 2H), 4.06 (d, 2H, ${}^{2}J_{PH}$ = 12.6 Hz, H4) ppm. ${}^{13}C\{{}^{1}H\}$ NMR (benzene- d_6 , 126 MHz, 25 °C) δ 145.9 (d, J= 3.1 Hz), 141.7 (d, J = 22.5 Hz), 126.5, 125.2, 124.5, 123.7 (d, J = 3.5 Hz), 56.8 (d, J = 18.9 Hz) ppm. $^{31}P\{^{1}H\}$ NMR (benzene- d_{6} , 162 MHz, 25 °C) δ 181 ppm. X- ^{15}N $^{31}P\{^{1}H\}$ NMR (benzene- d_{6} , 162 MHz, 25 °C) δ 181 (d, J_{PN} = 77.9 Hz), 181 (s, b) ppm. ¹⁵N NMR (benzene- d_6 , 50.7 MHz, 25 °C) δ 310, 197 ppm.

Synthesis of $[(dppe)Fe(Cp^*)(N_2)][BArF_{24}]$ (9). To a stirring solution of 100 mg (0.159 mmol) (dppe)Fe(Cp*)Cl in diethyl ether (4 mL) was added 141 mg (0.159 mmol, 1 equiv.) NaBArF₂₄ portionwise. After stirring for 60 min, the initially dark brown solution became pale red and a precipitate formed. The solution was filtered through Celite and the solvent removed from the filtrate. The red solids were triturated with pentane (3 x 2 mL) and dried under vacuum. The solids were dissolved in 2 mL diethyl ether and layered with 5 mL pentane to crystallize $[(dppe)Fe(Cp^*)(N_2)][BArF_{24}]$. After 24 h at room temperature large dark red blocks formed out of solution. These blocks were analyzed by NMR spectroscopy and in a X-ray diffraction crystallographic study. Yield: 173 mg (0.116 mmol, 73%).

Anal. Calcd for $C_{68}H_{51}BF_{24}FeN_2P_2$: C, 55.16; H, 3.47; N, 4.54. Found: C, 54.76; H, 3.84; N, 0.0 (we assume N_2 is eliminated upon heating). 1H NMR (diethyl ether (solvent suppressed), 500 MHz, 25 °C) δ 8.27 (m, 8H, BArF₂₄), 8.10 (m, found 14H, expected 16H), 8.03 (m, 4 H), 7.91 (m, 4H, BArF₂₄), 2.96 (m, 2H), 2.81 (m, 2H), 1.92 (s, 15H) ppm. $^{13}C\{^1H\}$ NMR (diethyl ether, 126 MHz, 25 °C) δ 162.1 (q, J = 50.0 Hz), 135.1 (m), 133.7 (m), 132.6 (m), 13.6 (d, J = 29.6 Hz), 130.9 (m), 129.6 (m), 125.0 (q, J = 272.0 Hz), 117.5 (m), 92.2 , 28.7, 9.0 ppm. $^{31}P\{^1H\}$ NMR (diethyl ether, solvent suppressed, 203 MHz, 25 °C) 85 ppm. IR (ATR, crystals covered with oil under air): 2117 cm $^{-1}$ (ν_{NN}).

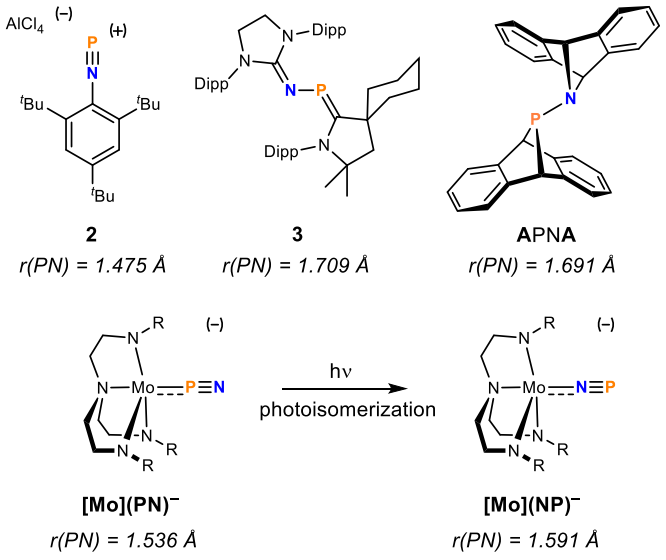
Synthesis of [(dppe)Fe(Cp*)(NP)][BArF₂₄] (10). Inside the glovebox, to a stirring solution of 55 mg (0.037 mmol) [(dppe)Fe(Cp*)(N₂)][BArF₂₄] in diethyl ether (5 mL) was added carefully 37 mg (0.148 mmol, ~4 equiv.) N₃PA portionwise. Gas evolution occured immediately and a precipitate (anthracene) develops. The solution was filtered after stirring for 15 min and placed in the freezer for 2 h to crystallize out any further anthracene. After two hours anthracene was filtered off and the resulting solution layered with 5 mL pentane to crystallize [(dppe)Fe(Cp*)(NP)][BArF₂₄]. After 24 h at room temperature large dark red blocks formed out of solution. These blocks were analyzed by NMR spectroscopy and in a Xray diffraction crystallographic study. Yield: 40 mg (0.027 mmol, 73%). C₆₈H₅₁BF₂₄FeNP₃: C, 54.53; H, 3.43; N, 0.94. Found: C, 54.20; H, 3.55; N, 0.34. ¹H NMR (diethyl ether (solvent suppressed), 400 MHz, 25 °C) δ 8.43 (m, found 9H, expected 8H, BArF₂₄), 8.20 (m, 20H), 8.01 (m, 4H, BArF₂₄), 3.31 (m, 2H), 3.01 (m, 2 H), 1.98 (s, 15 H) ppm. ${}^{13}C\{{}^{1}H\}$ NMR (diethyl ether, 126 MHz, 25 °C) δ 162.2 (q, J = 50.0 Hz, BArF₂₄), 135.3 (s (b), BArF₂₄), 133.8 (m), 133.6 (m), 132.7 (d, J= 29.6 Hz), 129.8 (m, BArF₂₄), 129.5 (m), 125.2 (q, J = 272.0 Hz, BArF₂₄), 117.7, 94.7, 28.1 (m), 9.0 (d, J = 29.6 Hz ppm. $^{31}P\{^{1}H\}$ NMR (diethyl ether, solvent suppressed, 203 MHz, 25 °C) 271 (t, J =9.2), 86 (d, J = 8.8) ppm. ¹⁵N enriched sample: ³¹P{¹H} NMR (diethyl ether, solvent suppressed, 203 MHz, 25 °C) 271 (dt, $J_{PN} = 53.4$, $J_{PP} = 9.5$), 86 (d, $J_{PP} = 8.5$) ppm. ¹⁵N NMR (diethyl ether, solvent suppressed, 50.7 MHz, 25 °C) δ 450 (d, J_{PN} = 51.1) ppm.

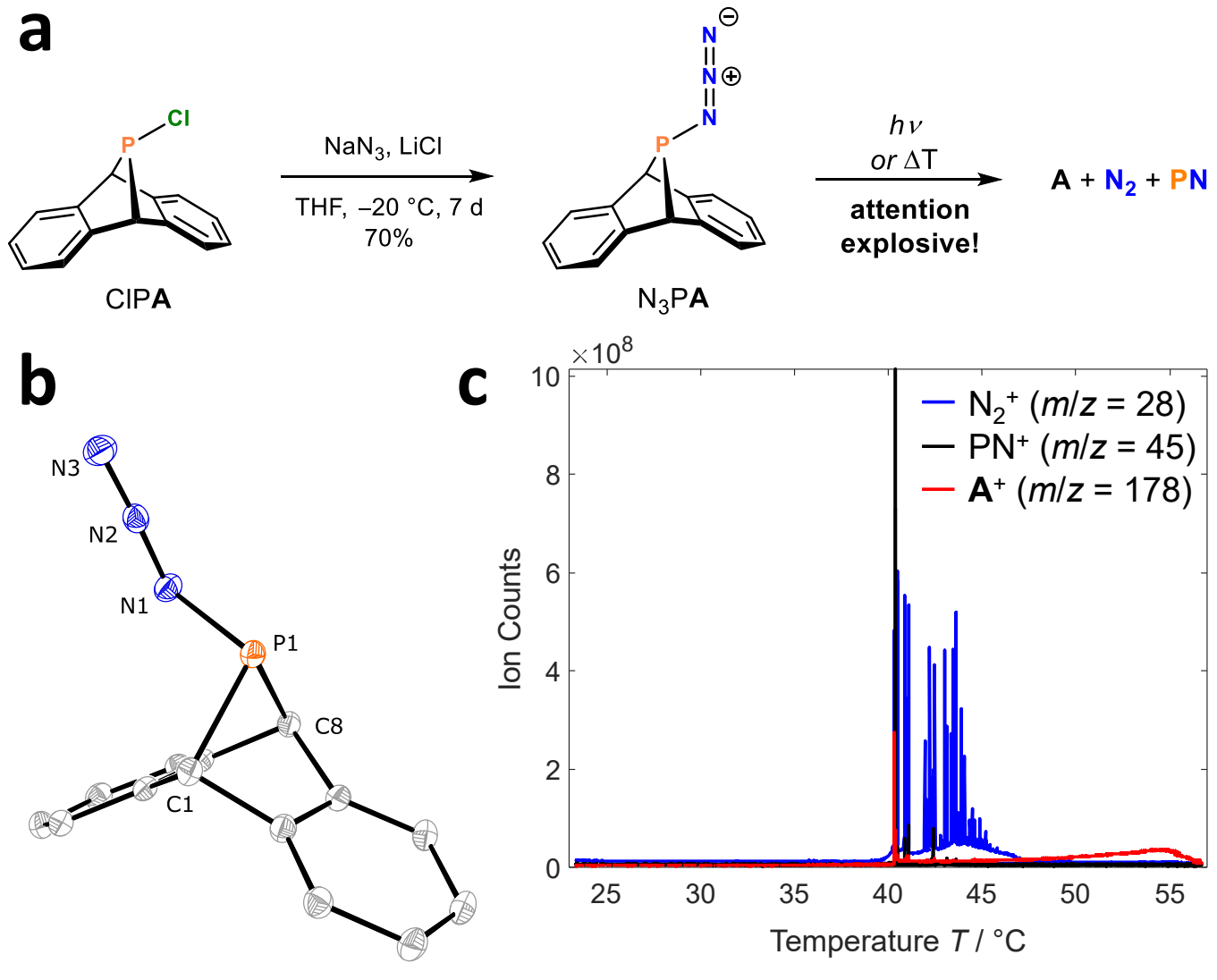
Data Availability

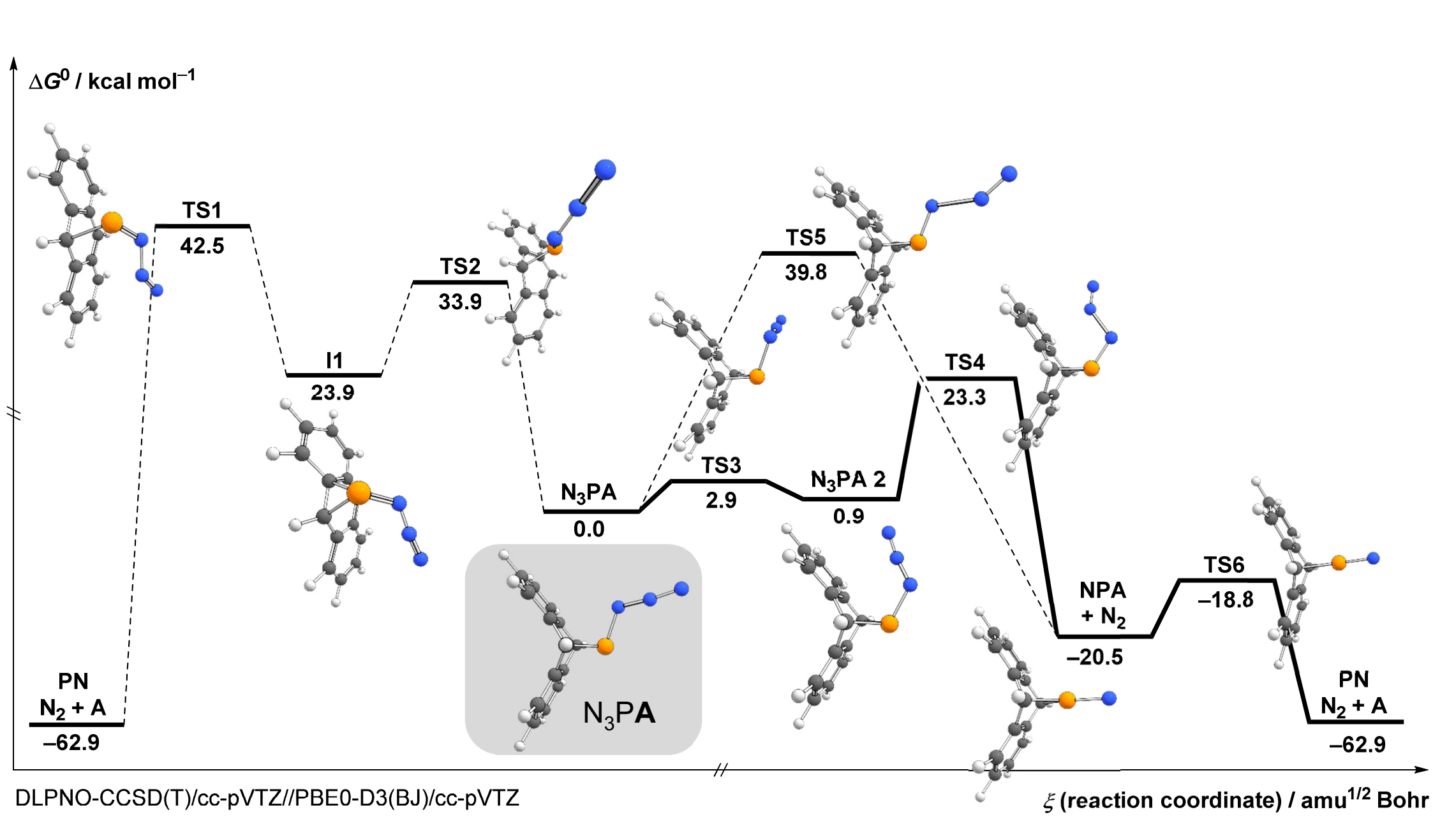
All relevant data generated and analyzed during this study, including crystal structures, NMR, IR, MBMS spectra and optimized coordinates for all calculated compounds, are included in this Article and its Supplementary Information, and are also available from the authors upon reasonable request. Crystallographic data for the structures reported in this Article have been deposited at the Cambridge Crystallographic Data Centre, under deposition numbers CCDC 2098667 (N₃PA), 2098666 (9) and 2098665 (10). Copies of the data can be obtained free of charge via https://www.ccdc.cam.ac.uk/structures/.

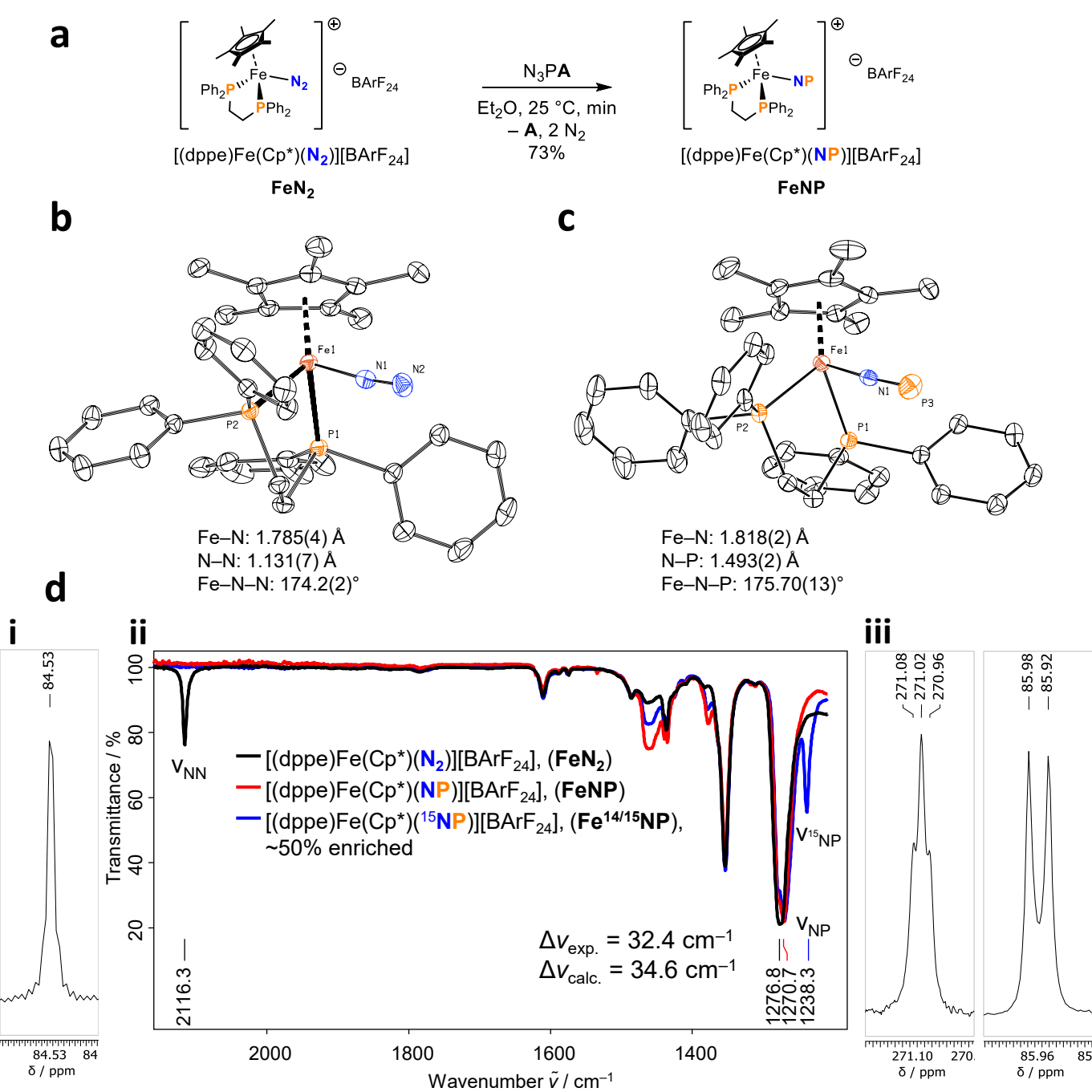
References

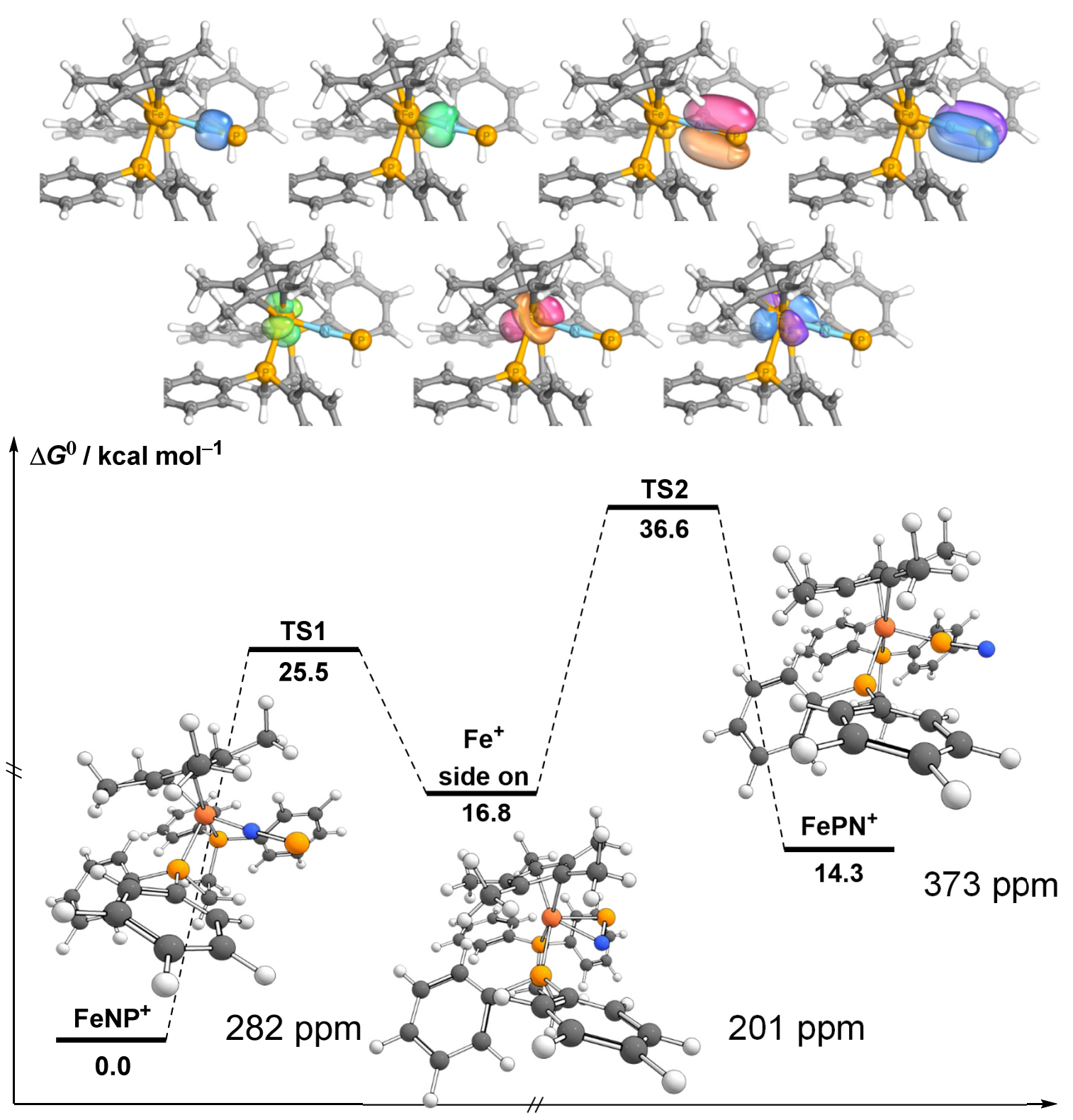
51. *Information on Azide Compounds; Stanford Environmental Health & Safety*, https://ehs.stanford.edu/reference/information-azide-compounds (accessed 08-24-2021).

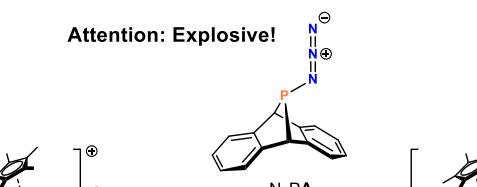
















FeNP